J. Fluid Mech. (1966), *vol.* 24, *part* 4, *pp.* 721–735
Printed in Great Britain

Natural convection in pools of evaporating liquids

By J. C. BERG† AND M. BOUDART‡
University of California, Berkeley
AND ANDREAS ACRIVOS
Stanford University

(Received 1 March 1965 and in revised form 15 September 1965)

In this exploratory study, schlieren photography has been used to reveal a variety of convection patterns in pools of evaporating liquids. Pure materials as well as binary solutions were investigated, both in the presence and absence of surface contamination, which was shown to exert a considerable influence on the convective flow. It was found that, with the exception of water, the observed flow structures were largely dependent on the depth of the evaporating pool and to a much lesser extent on the properties of the liquid. Also, it was possible to identify certain flow patterns as being induced by a surface-tension-driven instability and others as being due to buoyancy-driven convection; still other patterns seemed to be uniquely associated with the presence of surface contamination.

Introduction

Often, strange and interesting flow phenomena take place in 'quiet' pools of ordinary liquids undergoing evaporation, phenomena which go unnoticed generally when viewed with the naked eye. Nevertheless, it was over 100 years ago that James Thompson, a lecturer in civil engineering at Queen's College in Belfast and older brother of Lord Kelvin, first observed and reported on such flows in a note 'On Certain Curious Motions Observable at the Surfaces of Wine and Other Alcoholic Liquors', in which he attributed the evaporative convection to local variations in the surface tension (Thompson 1855). Later, in a letter in 1882 'On a Changing Tesselated Structure in Certain Liquids', he described the convection pattern in a tub of soapy water cooling in the yard of a roadside inn, and explained the observed motion as being due to the buoyancy forces resulting from evaporative cooling (Thompson 1882).

Both the surface tension mechanism, to which Thompson attributed the twitching and 'tearing' of strong wine, and the buoyancy mechanism, to which he attributed the plunging of cooled surface liquid along lines forming a 'tesselated' network in the scum on a tub of soapy water, are thought today to be appropriate. These are discussed in detail by Berg, Boudart & Acrivos (1966) and by Scriven & Sternling (1960). It suffices to remark here that both these mechanisms depend on the fact that evaporation cools the liquid surface,

† Present address: University of Washington, Seattle.
‡ Present address: Stanford University.

thereby increasing the surface tension as well as the density and leading in each instance to a potentially unstable stratification of the fluid. Such an unstable configuration may also be created of course by desorbing the component of lower surface tension or lower density from a binary solution, or by artificially heating non-evaporating liquids from beneath and allowing them to cool at the top. As a matter of fact, it was in this latter fashion that Bénard produced his celebrated polygonal convection patterns in thin layers of melted spermaceti (Bénard 1901; see figure 1, plate 1) which then motivated the linear hydrodynamic stability analyses of Lord Rayleigh (Strutt 1916), and later Jeffreys (1928), Low (1929), Pellew & Southwell (1940) and Pearson (1958), to name but a few, that were aimed at predicting theoretically both the necessary conditions for the onset of convection in horizontal fluid layers and the 'cell size' that the developed flow patterns would assume.

It is well known by now that there have been several cases where the linear theory has met with success in predicting quantitatively the stability criterion. This is in contrast to the question of 'cell size', where the 'agreement' between theory and experiment has been little more than occasional or coincidental. Of course, this failure is not surprising, since the use of a linear analysis for describing fully developed flows is indeed highly questionable. In addition, however, the development of a more meaningful theory for such convective flows is severely hampered by the scarcity of much detailed experimental knowledge regarding the various flow patterns that occur in evaporative cooling. Thus, for example, as Thompson's early observations themselves demonstrated, these convective flows are not always cellular, so that the question of 'cell size' is often without much meaning.

To be sure, in addition to the theoretical effort, Bénard's work also stimulated a number of experimental studies, but most of these involved rather specialized cases of fluids heated from below. Notable, though, is Dauzère's work with melted wax, which suggested that, besides 'cells' and 'tesselations', several other non-cellular flow structures were possible, and that small amounts of surface contamination could affect profoundly the convection pattern (Dauzère 1912, 1913). Even more pertinent for our purposes, however, is Spangenberg & Rowland's (1961) study of flow patterns in deep tanks of water undergoing evaporation, where the presence of Thompson's 'tesselations' was dramatically confirmed photographically by means of an ordinary schlieren technique, which thus emerged as a convenient and valuable experimental tool for investigating the morphology of evaporative convection.

In the present work, schlieren optics were used to reveal a variety of flow patterns in an evaporating liquid layer. The work was undertaken to obtain qualitative information concerning both the structure and the scale of these flows, and particularly the manner in which they are affected by fluid properties, fluid depth, and the presence of surface contamination, since it appears that such a study must precede the development of any sound theory regarding the behaviour of these flow systems. Experiments were performed with acetone, benzene, carbon tetrachloride, *n*-heptane, isopropanol, methanol, and water, as well as with a number of binary solutions from which one component was

desorbed. The materials were evaporated into still air from liquid layers 10×10 cm in horizontal extent and with depths ranging generally from 0·25 to 10 mm.

Aside from its fundamental interest, this subject is also of particular importance to chemical engineers for the reason that a complete understanding of evaporative convection, i.e. one's ability to predict its occurrence, its form, and its intensity, together with the appropriate coefficients for heat and mass transfer, would aid in the design of many fluid-phase contact devices such as those which are encountered in distillation, absorption, and liquid–liquid extraction.

Experimental procedure

A 10 cm cubical evaporation vessel, as shown in figure 2(*a*), was first used in this work. The bottom and a pair of opposing sides contained windows of $\frac{1}{8}$ in.-thick optically flat glass. The top was open, and the effective depth of the

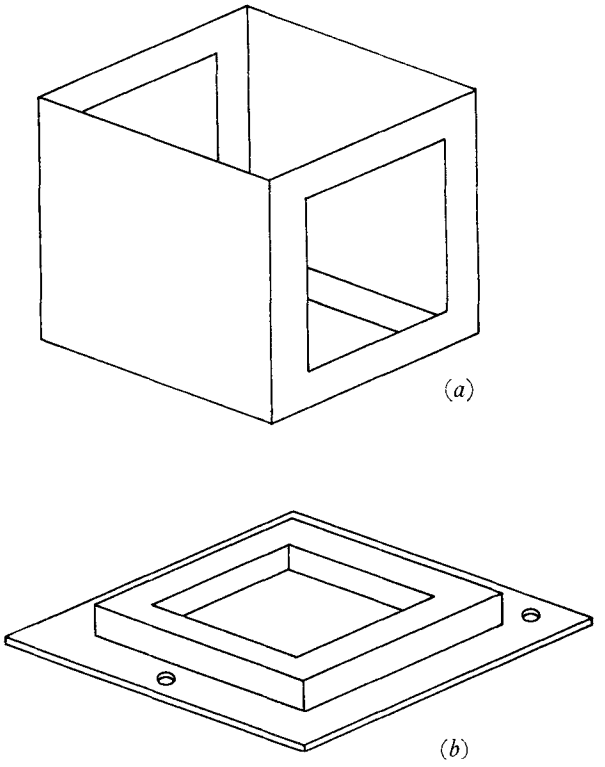

FIGURE 2(*a*). Evaporation vessel used for deep liquid layers.
(*b*) Evaporation vessel used for shallow liquid layers.

evaporating liquid was set by adjusting the level of a horizontal glass plate beneath the surface. However, since it soon became apparent that in none of the cases under study did the convection patterns change when the depth was increased beyond a value of approximately 1 cm, a more convenient shallow evaporation vessel, shown in figure 2(*b*), was used for most of the work.

The flow patterns in the evaporating layers were observed using a conventional schlieren technique, which permits one to see and to photograph gradients of refractive index (and hence gradients of temperature and composition) in a transparent medium. The method has been described already in great detail (Schardin 1947; Holder & North 1956). Nevertheless, we shall digress here briefly in order to outline the basic principles of the schlieren method, and, in particular, to explain how flow patterns in evaporating liquid pools may be deduced from schlieren photographs.

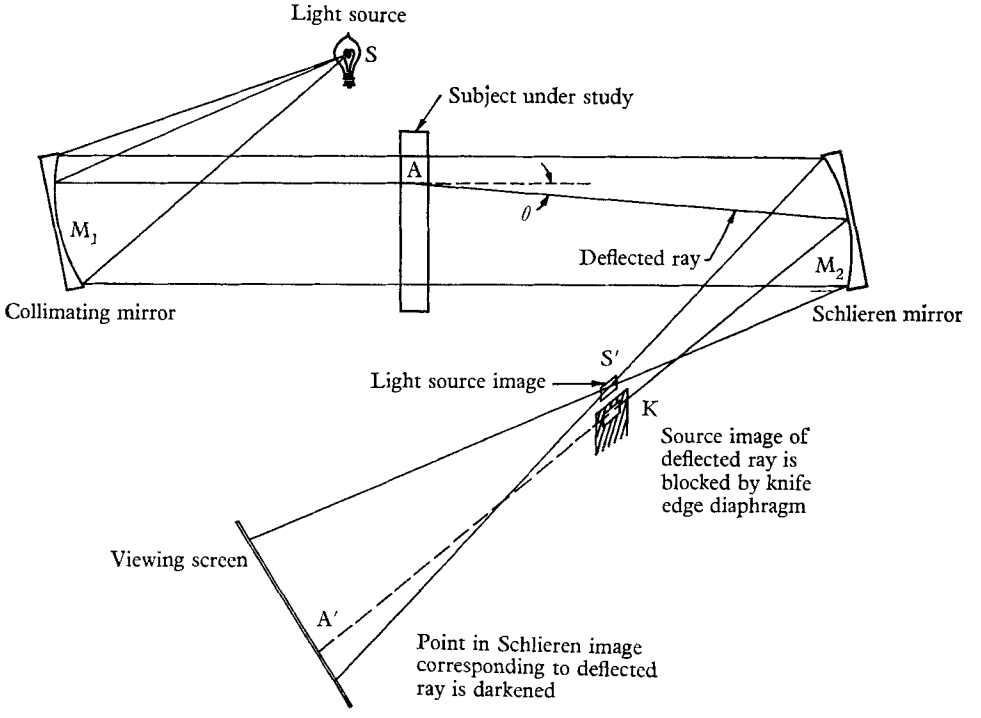

FIGURE 3. Schlieren system constructed from a pair of parabolic mirrors. Diagram shows how schlieren image is formed on the viewing screen by blocking light rays which were deflected in passing through the subject under study.

The schlieren method employs light produced from a small but finite source S (see figure 3) of well-defined shape. In the present study, S was the horizontal ribbon filament of a tungsten lamp. The light emanating from S is condensed by either a convex lens or a concave mirror into a parallel or nearly parallel beam that is subsequently intercepted by a second lens or mirror which refocuses it into an image S′ of the original light source S. The arrangement used in the present work, in which a pair of parabolic mirrors M_1 and M_2 was employed, is shown in figure 3.

The transparent subject to be studied is inserted into the light beam between the mirrors M_1 and M_2, and a viewing screen is located at such a position that an image of the subject is brought to focus upon it. The presence of the transparent subject, which, in the present work, was a pool of evaporating liquid, affects but little the formation of the source image S′, but the slight perturba-

tion that it does produce is the essential feature of the schlieren method. Consider the origin and make-up of the source image S′: The source S, itself, casts light upon the collimating mirror M_1 so that each point on the surface of M_1 receives light from *all* points of the source S. Each individual ray of light emerging from the surface of M_1 thus contains light from all points of the source S, and upon being refocused by M_2, is capable of reproducing an image of S. Hence, each ray of light produces its own source image, and the final image S′ is obtained by the exact superposition of all these individual images.

Now, the precise superposition of the individual source images to produce the final image S′ is disrupted if any of the light rays are deflected in travelling from M_1 to M_2, and such deflexions do indeed occur if the beam is made to traverse a medium in which the refractive index varies from point to point. In particular, the magnitude of the angular deflexion θ of a given ray is directly proportional to the gradient of the refractive index at point A in the subject, and, if as shown in figure 3 the deflexion is negative, the source image produced by this ray will lie below the image produced by those rays which are not deflected. Similarly, rays may experience upward or lateral deflexions. Even though they may be deflected, however, these rays go on to form an unaffected image of the subject on the viewing screen, each ray, regardless of its deflexion, forming the point in the image corresponding to the point at which it traversed the subject.

The essence of the schlieren method consists in making these refractive index variations visible on the screen. This is accomplished, as shown in figure 3, by blocking, wholly or partially, deflected rays by means of a diaphragm placed at S′. Image points corresponding to rays that are deflected downward will thus appear as darkened spots on the viewing screen. Often, the diaphragm is a simple knife edge arranged to block off about half the undeflected light so that both upward and downward deflexions may be detected on the screen. All rays experiencing the same deflexion θ yield image points that are darkened (or brightened if the deflexion is upward) equally on the viewing screen, and, regardless of the amount of deflexion, a ray emerging from a given point A in the subject always produces an image at the same corresponding point A′ on the screen. Thus, the schlieren image is a pattern of light and dark regions constituting a map of the refractive index gradient within the transparent subject under study.

It should be noted that, in the present work, the knife-edge diaphragm was oriented horizontally so that only vertical deflexions could be detected, and the resulting schlieren image mapped the variation of refractive index in the y-direction (perpendicular to the direction of the light rays) shown in figure 4 (plate 2).

Since the refractive index of a fluid is a function of its temperature and, in the case of solutions, of composition, the schlieren method can be used to visualize the distribution of temperature or composition in a liquid pool. Furthermore, since an evaporating liquid will have generally a non-uniform temperature distribution owing to the presence of convective flow, the method may be used to visualize flow patterns in such systems.

In the present study, a 6 in. two-mirror system was employed as shown

schematically in figure 3. The light source was a 105 W tungsten ribbon lamp with a horizontal filament 2×8 mm in size. The mirrors had a focal length of 4 ft. and were placed 12 ft. apart. The parallel beam of light emerging from the collimating mirror was made to pass through the evaporating layer from top to bottom (thus yielding a top view of the flow) by an arrangement of plane mirrors shown in figure 5. The knife-edge diaphragm consisted of a blackened razor blade mounted to the vernier from an adjustable microscope stage, and the schlieren image was brought to focus on the $3\frac{1}{4} \times 4\frac{1}{4}$ in. photographic plate of a Graflex (series B) single-lens reflex camera, the camera lenses of which had been removed.

A typical run was made by pipetting a given amount of liquid into the vessel, covering it with a glass plate and placing it in the schlieren beam. When all evidence of fluid motion was absent, the cover was slid from the vessel and the liquid was observed through the reflex mechanism of the camera. Usually within 5 sec a convection pattern appeared which, within 15 sec, stabilized into a quasi-steady form. The photographs to be reported here are top views of this 'steady' form taken 30 sec after evaporation had begun.

Qualitative interpretation of the schlieren image

Consider a shallow pool of evaporating liquid to be placed in the collimated light beam of a schlieren system so that, as shown in figures 4 (plate 2) and 5, the light traverses the pool from top to bottom.

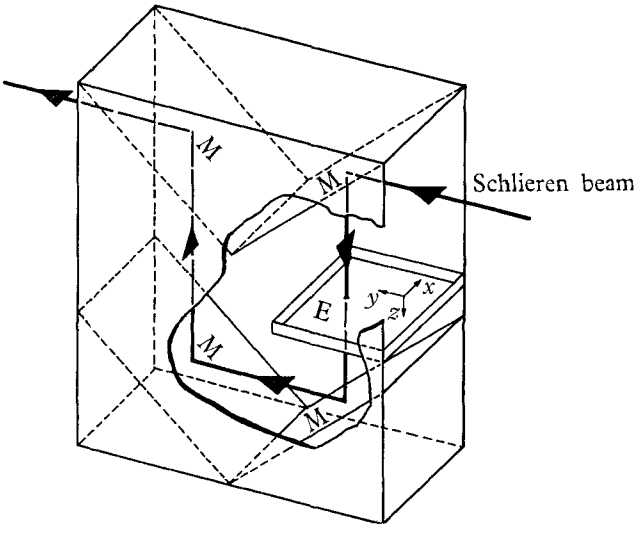

FIGURE 5. Mirror arrangement used to obtain a horizontal view of the evaporating liquid layer. M, plane front surface mirrors; E, evaporating liquid.

An example of a schlieren image (produced from a 2 mm deep pool of evaporating methanol) is depicted in figure 4 (plate 2). Points of equal brightness in the image correspond to points of equal refractive index-gradient in the evaporating liquid pool. More precisely, the image brightness at a given point is

linearly related to the integral average of the y-component of the refractive-index gradient over the depth of the pool, i.e. to

$$\frac{1}{h}\int_0^h \left(\frac{\partial n}{\partial y}\right) dz,$$

where h is the depth of pool and n is the refractive index; z is the vertical co-ordinate, x the co-ordinate parallel to the knife edge. Thus a field of uniform refractive index, i.e. zero gradient, yields an image of uniform (mean) brightness.

The depth of field for the system was approximately 2 in., so that the top views shown in this work depict conditions within the entire thickness of the liquid rather than the surface layer alone. The patterns in the photographs thus represent integrated refractive index variations *within* the evaporating layers, so the apparent ridges and troughs in these schlieren images do not necessarily represent the actual relief of the evaporating surfaces, even though such surfaces do exhibit in general a slight relief† when convection is taking place.

The entire image, being a map of the plan form distribution of the (depth average) refractive index gradient, is also a map of the (depth average) temperature gradient $\partial T/\partial y$ in the evaporating liquid since, for pure liquids, the refractive index is a (monotonically decreasing) function of the temperature. At point R (figure 4) the refractive index gradient is zero, and, at the corresponding image point R′, the image is of medium (or mean) brightness as is the case with undeflected rays. Now consider the variation of the image brightness in a thin strip P′Q′ of the schlieren image (figure 4) corresponding to a strip of the liquid layer PQ. Points along this strip brighter than R′ correspond to points where the refractive-index gradient is positive (temperature gradient is negative), producing an upward deflexion of the rays over the knife edge. Conversely, darker points indicate a positive $\partial T/\partial y$. Therefore, as shown in figure 4, one can construct a qualitative plot of light intensity *vs* position along this strip to produce a curve of $\partial T/\partial y$ vs y, which in turn may be integrated graphically to yield the depth-mean temperature distribution T along y. It is evident from figure 4 that temperature extrema occur in the fluid at points corresponding to abrupt changes in intensity in the image such as at points 1, 2, 3 and 4. It is further evident that, in moving from P′ to Q′ (i.e. in the positive y direction), an abrupt change from dark to light, such as point 4, corresponds to a temperature maximum, whereas an abrupt change from light to dark indicates a temperature minimum. Thus, by considering all strips of fluid such as PQ, one should be able to construct a qualitative temperature map over the entire horizontal plane, and to identify the lines dividing light from dark regions in this map as either 'hot' or 'cold'.

In all the photographs of this paper, the positive y direction is as shown in figure 6 (plate 1), so that 'hot' lines have the bright area above and the dark area below, and conversely for 'cold' lines. The temperature distribution shown in figure 4 (plate 2) forms thus a cellular pattern with warm fluid within the cells and cold fluid along the cell partitions.

† Interferometric studies with melted spermaceti, whose properties differ somewhat from those of the liquids in the present work, have indicated that differences in surface elevation during such convection are typically of the order of one micron (Bénard 1901).

Having obtained a qualitative temperature distribution from the schlieren image, one may then deduce† the qualitative features of the corresponding flow structure. In the example of figure 4, warm fluid is evidently flowing toward the surface at each cell centre, spreading outward over the surface where it is cooled, and then returning to the interior of the pool along the cell periphery. Thus, each cell constitutes a torus shown schematically in figure 8. The indicated temperature distribution cannot be supported of course by flow in the opposite direction, i.e. upward along the cell partitions and downward at the cell centres, since this would imply that a fluid element is warmed instead of cooled as it moves across the surface.

Non-cellular flow structures can also be deduced from schlieren pictures in the same way. On the other hand, when liquid solutions are studied, a simple interpretation of the schlieren photographs cannot be made in general in the manner outlined above, since the refractive index is a function both of composition and temperature. More detailed discussion of the interpretation of schlieren images is to be found in Schardin (1947), in Holder & North (1956) and in Berg (1964).

Convective patterns as a function of liquid depth

Typically, evaporative convection in pure liquids consists of three basic structural forms of flow. These are illustrated in figures 7 (*a*)–(*f*) (plate 3), which show top views of evaporating benzene (a 'typical' liquid with respect to its evaporative convection) in pools of increasing depth. Cellular flow, as depicted in figure 7 (*a*), was first to make its appearance. As the photographs suggest, this flow is qualitatively the same as that observed by Bénard in thin layers of spermaceti, and consista of warm fluid from the interior of the pool rising to the surface at each cell centre, and then returning to the interior, along the cell partitions, as cooled liquid. Each cell, shown diagrammatically in figure 8, constituted a small torus independent of the other cells.

As the depth of the pool was increased from 0·5 mm the overall cellular pattern persisted but, as expected, there was a marked increase in the size of the cells. In addition, other changes in the flow became apparent. Beginning at the 3 mm depth, figure 7 (*c*), but particularly at the 4 mm depth, figure 7 (*d*), there was evidence of the second structural flow form, superimposed on the background pattern of cells, which appeared in the top views as a cross-hatching of the cells with fine lines, termed 'ribs'. In contrast to the cell network, which remained almost stationary with time, the ribs moved about rapidly and disappeared by collapsing into a cell partition, with a single rib generally existing for less than a second. The ribs themselves, like the cell partitions, represented lines where cool fluid would plunge from the surface into the interior.

Even if the ribs are removed from the cell pattern obtained at the 4 mm depth, figure 7(*d*), yet another structural change may be noticed. The upwellings of the warm fluid, which in shallower layers occurred in *columns* at the cell centres, were now beginning to occur along *lines* within the cells. Often several

† Using of course elementary consequences of continuity and buoyancy.

of these 'hot lines' would radiate from a cell centre outward to the cell periphery, as is evident in the lower right portion of figure 7 (*d*).

As the depth increased further, the ribs persisted and the cells began to transmute themselves into another pattern. The polygonal cell boundaries,

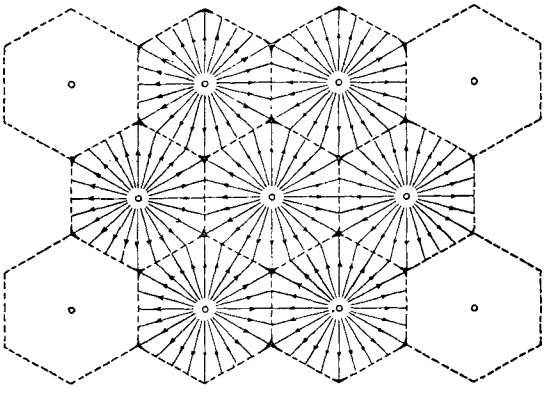

(*a*)

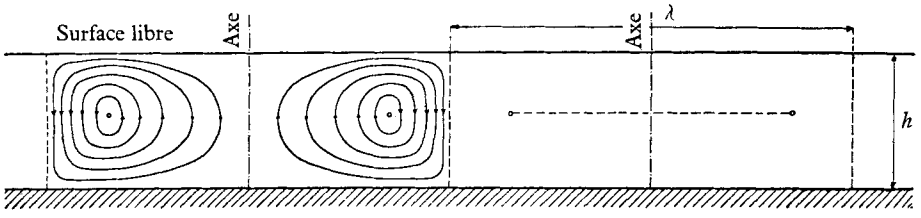

(*b*)

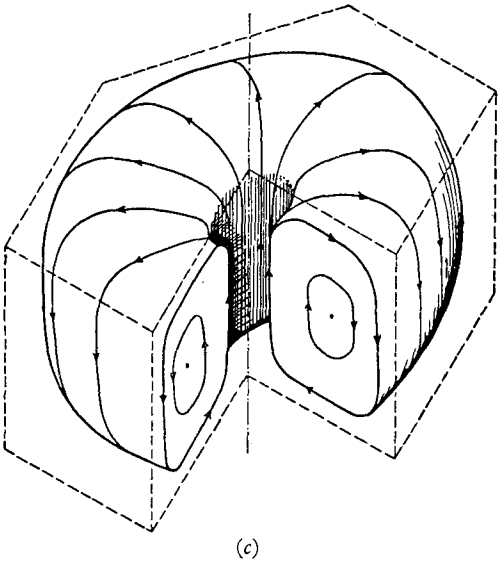

(*c*)

FIGURE 8. Steady cellular convection as observed by Bénard (Avsec 1939). (*a*) Top view; (*b*) side view; (*c*) perspective view.

which were very large and deformed when the depth had reached about $\frac{1}{2}$ cm, broke open, and they were no longer surrounding independent cells. Moreover, with further increase in depth, these former boundaries became 'cold lines' which wandered sluggishly about the surface. Meanwhile, the 'hot lines' had grown in length, so that the overall pattern was that of a loose network of 'hot lines' and 'cold lines' both of which might appropriately be called 'streamers'. Along these lines warm fluid rose and cold fluid fell, respectively, in sheet-like plumes. Figure 9 (plate 4) shows the fully developed pattern of streamers, interspersed with ribs, at a depth of 1 cm, beyond which no further changes in flow form could be discerned.

Since evaporative convection in pure liquids is due solely to surface cooling, an attempt was made to determine experimentally the approximate temperature gradient along the evaporating surface. This was accomplished by means of direct temperature measurements with a thermocouple which indicated that, for depths in excess of 3 mm, a surface temperature difference of the order of 1 degC existed between the cell centres and the cell boundaries, or between the hot streamers and the cold streamers. However, such measurements were difficult to obtain and to interpret because the thermocouple surrounded itself with a curved meniscus which greatly distorted the schlieren image, and because the presence of the thermocouple tended to affect the convection itself. Thus it was impossible to obtain meaningful measurements for the small structures such as those prevailing at depths less than 3 mm.

Effect of fluid properties

It has been asserted that benzene is a 'typical liquid' with respect to its evaporative convection. This is indeed so, for, although liquids representing a considerable range of properties were investigated, it was found that the metamorphosis with depth from the small regular cells to the larger cells in which a substructure of ribs appeared, followed by the dismemberment of the cells into a network of sluggishly moving hot and cold streamers, was qualitatively the same for all of the liquids except water. The fluids which were studied, together with some of their properties, are shown in table 1. All these materials were of reagent grade, and no attempt was made to purify them further. The chief difference between their various convection patterns was that, for a given depth, the horizontal size of the structure (such as the cell diameter) varied somewhat from one liquid to another, although no quantitative correlation could be established between the size and any particular fluid property. Low viscosity and low surface tension seemed to favour the formation of larger cells at a given depth. Figures 10(*a*)–(*h*) (plates 5 and 6) show a comparison of cellular flows in the various liquids at a depth of 1 mm. Note that ribs are already in evidence in acetone.

In addition to varying cell size, the particular depth at which a given structural form made its appearance (cells, ribs, streamers) was not precisely the same for all of the liquids. However, in all cases except water, all of the three flow régimes occurred at one depth or another and the same fully developed pattern was found to exist when the depth reached 1 cm.

The effect of increasing the evaporation rate was investigated qualitatively by passing streams of dry nitrogen laterally over the surface at rates up to 2 l./min. The flow patterns were quite stable to this moderate blowing. It was found that this caused a slight decrease in the cell size for a given depth and a sharpening of the cell boundaries if the prevailing convection was cellular, and a slight increase in the number of hot and cold lines per unit area if the régime was one of streamers.

Material	Surface tension	Density†	Viscosity	Thermal expansion coefficient	Thermal conductivity†	Evaporation rate in still air‡
Acetone	23·7†	0·729	$0{\cdot}326 \times 10^{-2}$†	$1{\cdot}487 \times 10^{-3}$†	$4{\cdot}543 \times 10^{-4}$	$0{\cdot}56 \times 10^{-6}$
Benzene	28·8†	0·879	0·652†	1·237†	3·780	0·32
CCl_4	26·9†	1·463	0·969†	1·236†	2·470	0·28
Dioxane	33·5§	1·035	1·351§	—	—	0·17
Heptane	20·3§	0·684	0·409†	1·240§	3·354	0·17
Isopropanol	21·4†	0·785	2·60†	1·41§	3·362	0·23
Methanol	22·6†	0·793	0·597†	1·199§	4·832	0·37
Water	73·0†	0·998	1·005†	0·207†	14·29	0·15

All quantities reported in c.g.s. units for a temperature of 20 °C.

† *Handbook of Chemistry and Physics*, 38th edn. (1956–57).

‡ Measured in this laboratory.

§ *International Critical Tables.*

TABLE 1. Properties of materials studied

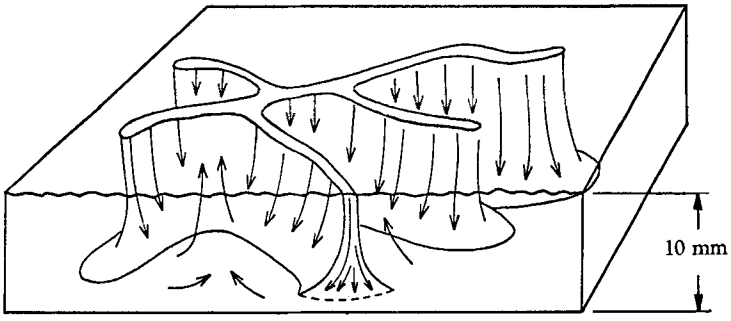

FIGURE 12. Evaporative convection in cold streamers. Cold fluid plunges along distinct lines in the surface and warm fluid rises slowly in the area between the streamers.

Water

Water did not behave like the other fluids. No convection at all was evident until the depth reached about 1 cm, and at that depth (and beyond) the pattern was one of cold streamers alone, as shown in figure 11 (plate 7) and diagrammed in figure 12. This pattern, which differed from that of figure 9 (plate 4) in that ribs were totally absent, was the same as that described by Thompson (1882) and photographed by Spangenberg & Rowland (1961), who also noted the absence of convection at depths less than 1 cm. As discussed below, this 'anomalous' behaviour of water may be due in part to surface contamination by means of surface-active agents.

Surface contamination

In order to determine the effect of 'contamination' on the morphology of the evaporative convection, oleic acid, hexadecanol (both typical surfactants on water), and paraffin wax (a suspected contaminant in some previous runs with 'pure' liquids) were added to the various evaporating liquids in amounts varying from 0·5 mg to 3 g/l. It was expected that such materials would be forced to concentrate in the surface layer during the evaporation of the solvent, thus forming a crust which was sometimes visible to the naked eye and which did indeed exert a profound influence on the convective flow patterns.

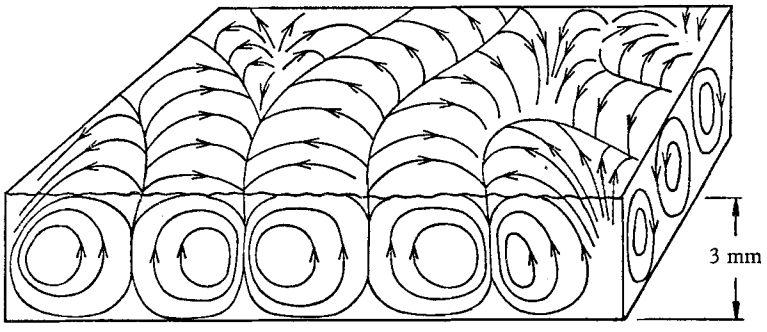

FIGURE 15. Evaporative convection in vermiculated rolls. Cold fluid flows down in a relatively narrow region near the roll partition while warm fluid rises over a wider, less distinct region. As fluid depth is increased the warm partitions lose their identity, and the cold partitions become streamers.

As was the case for pure liquids, the developed flows in liquid layers with contaminated surfaces underwent a metamorphosis as depth was increased, a metamorphosis which was qualitatively independent not only of the evaporating material (except for water) but also of the particular contaminant. Usually no convection at all occurred at depths of 1 mm or less, except for the infrequent occurrence of some isolated cells as shown in figure 13 (plate 12), but, as the depth was increased to 2 mm, convection occurred in a new form, in two-dimensional, worm-like roll cells shown in figure 14 (plate 8) and diagrammed in figure 15. As expected, the width of these 'vermiculated' roll cells increased with increasing depth, but, as shown in figures 16(*a*)–(*e*) (plate 9), ribs were totally absent. Also, as depth increased, the cold lines became more distinct while the hot lines grew more diffuse until finally, when the depth had reached 8 or 9 mm, only cold lines were evident, as in figure 16 (*e*), and the structure became the same as that observed in water. Finally, it is interesting to note that the cold streamers in water were not affected perceptibly by the addition of contamination.

A striking feature of the contamination effect was the small amount of contaminant required to produce the results which have been described. 0·5 mg/l was usually sufficient, and often the materials became contaminated accidentally by, presumably, trace amounts of impurities. Attempts to produce

'partial contamination' by adding ever smaller quantities of a given 'impurity' never produced a hybrid flow pattern, but occasionally resulted in what Hickman (1952) has called a 'schizoid surface', in which parts of the surface were covered with a film while others were clean. An example is shown in figure 17 (plate 10).

As mentioned earlier, the presence of impurities in unavoidable trace amounts may furnish a possible explanation for the unique behaviour of water during evaporation. Thus, for water, there is not only the possibility of having contaminants in the form of a crust sustained by evaporation, as with the systems just described, but there is also the possibility of having materials present which are 'surface active' in the classical sense, i.e. preferentially residing in the surface region even in the absence of evaporation and capable of substantially reducing the surface tension. Such materials generally consist of large hydrophobic organic molecules possessing a hydrophilic functional group, such as oleic acid and hexadecanol. In a recent hydrodynamic stability analysis (Berg & Acrivos 1965), it was shown theoretically that the presence of even trace amounts of such contamination, i.e. as low as 10^{-9} mole/cm^2 of surface or less than 1/100 of the amount needed to form a close-packed monolayer, should be expected to stabilize a water layer up to a depth of the order of 1 cm by effectively removing the surface tension mechanism for evaporative convection, thereby leaving the buoyancy mechanism as the only vehicle for setting the fluid in motion.

Two experimental observations tended to corroborate this explanation for the 'anomalous' behaviour of water. First, the convection that *did* develop in water when the depth had reached 1 cm was of the type associated with the presence of contamination; i.e. it consisted of cold streamers without any ribs. Secondly, in contrast to the other materials studied, no noticeable change was produced when surfactant contamination was intentionally added to the water, thereby suggesting that the surface had already been contaminated to a degree sufficient to alter the convection.

The dependence of the morphology on the driving mechanism

In general, in an evaporating pure liquid, the convective pattern is brought about by both a buoyancy and a surface tension driving force, so that, by looking at pure liquids alone, it is not possible to examine the flow structure that is associated with either mechanism in the absence of the other. However, this point, which is an interesting one since the buoyancy and surface tension mechanisms are fundamentally quite distinct, can indeed be investigated at least partially by studying the flow patterns accompanying desorption from a binary solution.

To illustrate how this can be accomplished, consider the mixture of 1,4-dioxane and water. The experiment was performed by saturating the vapour above the solution with water. As a result, there was, at first, some condensation of water into the solution while dioxane was being desorbed. As the dioxane desorption proceeded, however, the surface layer became essentially pure water and further condensation of water vapour did not take place. In this manner then, a liquid

layer was formed which was not only somewhat cooler at the top than in the interior, but was also much leaner in dioxane near the surface than in the bulk.

The density of dioxane relative to water is 1·03, whereas the surface tension of dioxane is 33·5 dyn/cm compared with 73 dyn/cm for water. Thus, the surface tension of the water-rich upper layer would be higher than that of the dioxane-rich bulk, thereby leading to a potentially operative surface tension mechanism. On the other hand, the situation is quite different with respect to the buoyancy mechanism. Surface cooling (which according to our measurements produced a drop in surface temperature of less than 1 degC in this case) increases the density by about 0·2 %, but this is more than offset by the dioxane depletion near the surface which *decreases* the density by about 3 %. As a consequence, the net effect of the dioxane evaporation is to produce a *surface* layer of fluid *lighter* than that beneath, which is of course stably stratified with respect to density. Thus, any convection in this situation could be attributed with confidence to the surface tension mechanism. In contrast, when the desorption was reversed, i.e. when water was desorbed from the same dioxane–water solution, it was the buoyancy mechanism which became potentially operative.†

As will be illustrated presently, the experimental results did indeed show marked differences in the convection patterns as produced by the two mechanisms. For the surface tension case, i.e. for dioxane desorbing from water, we first obtained, at 1 and 2 mm, a series of independent upwellings of fluid which grew to diameters of about 0·5 cm as shown in figure 18(*a*) (plate 11), then shrank and vanished, to be replaced by others. As the depth was increased (see figures 18(*a*)–(*d*), plate 11) these upwellings grew in size, impinged upon one another and finally developed a fine-grained and very active internal sub-structure. When the depth was more than 5 or 6 mm, the upwellings encompassed the entire 100 cm^2 area of the surface, and the entire structure was one of chaotically moving fine streamers which increased in number and activity as the depth reached about 1 cm, beyond which no further change could be detected. Trace amounts of contamination completely removed all convection at all depths. Moreover, it appeared that some contamination was present in all the solutions since, if one waited long enough (usually from 5 to 15 min), part of the surface would become inactive as shown in figure 19 (plate 12). Eventually, the inactive region would spread to the whole surface.

In contrast, when the desorption was reversed, i.e. when water was desorbed from dioxane, the results were dramatically different. No convection at all was observed until the liquid depth reached about 1 cm, and then the resulting pattern was one of almost stationary streamers as shown in figure 20 (plate 13). These streamers persisted indefinitely, and were unaffected by the addition of surface contamination.

Generally, binary solutions from which one component is desorbing may be divided into four categories:

(1) Those susceptible to both buoyancy and surface tension convection.

† In both cases, of course, the inoperative mode would be expected to exert a stabilizing influence on the operative mode; i.e. one would expect the buoyant forces to retard the surface-tension-driven flow and conversely.

(2) Those susceptible to surface tension convection only.

(3) Those susceptible to buoyancy convection only.

(4) Those susceptible to neither surface tension nor buoyancy convection.

Runs were made with all four types (Berg 1964). In qualitative terms the expected results were always obtained, in the sense that convection in some form occurred when the solution was susceptible to either or both of the convective mechanisms, but never for the type (4) solutions. However, some of the observed patterns, such as those shown in figures 21–24 (plates 14 and 15), were truly bizarre (and puzzling!).

Surface contamination exerted a perceptible influence only on solutions of types (1) and (2), and was particularly effective in the case of aqueous solutions. Solutions in which the buoyancy mechanism alone was operative showed no effect of contamination, and solutions of type (4) exhibited no convection at all under any conditions.

In summary then, schlieren photography has revealed a variety of patterns in evaporative convection. Several flow forms have been systematically associated with different depths of the fluid layer, and the presence of small amounts of surface contamination has been shown to have a profound effect on the morphology of the developed convection in those cases where the surface tension mechanism played an important role.

This work was supported in part by a National Science Foundation fellowship to J. C. Berg, by the Office of Saline Water and by the Petroleum Research Fund administered by the American Chemical Society.

REFERENCES

AVSEC, D. 1939 *Publ. Sci. & Tech. du Min. de l'Air*, **155**.

BÉNARD, H. 1901 *Ann. Chim. Phys.* **23**, 62.

BERG, J. C. 1964 Ph.D. Thesis, University of California, Berkeley.

BERG, J. C. & ACRIVOS, A. 1965 (to appear in *Chem. Engng Sci.*).

BERG, J. C., BOUDART, M. & ACRIVOS, A. 1966 *Advanc. Chem. Engng*, **6** (to be published).

DAUZÈRE, C. 1912 *C.R. Acad. Sci., Paris*, **154**, 974; **155**, 394.

DAUZÈRE, C. 1913 *C.R. Acad. Sci., Paris*, **156**, 218, 1278.

HICKMAN, K. C. D. 1952 *Ind. Engng Chem.* **44**, 1892.

HOLDER, D. W. & NORTH, R. J. 1956 Optical methods for examining the flow in high speed wind tunnels. *NATO AGARD Rep.*

JEFFREYS, H. 1928 *Proc. Roy. Soc.* A, **118**, 195.

LOW, A. R. 1929 *Proc. Roy. Soc.* A, **125**, 180.

PEARSON, J. R. A. 1958 *J. Fluid Mech.* **4**, 489.

PELLEW, A. & SOUTHWELL, R. V. 1940 *Proc. Roy. Soc.* A, **176**, 312.

SCHARDIN, H. 1947 Toepler's schlieren method; basic principles for its use and quantitative evaluation. *The David Taylor Model Basin, U.S. Navy, Trans.* no. 156.

SCRIVEN, L. E. & STERNLING, C. V. 1960 *Nature, Lond.*, **187**, 186.

SPANGENBERG, W. B. & ROWLAND, W. R. 1961 *Phys. Fluids*, **4**, 743.

STRUTT, J. W. S. (Lord Rayleigh). 1916 *Phil. Mag.* (6) **32**, 529.

THOMPSON, J. J. 1855 *Phil. Mag.* (4) **10**, 330.

THOMPSON, J. J. 1882 *Proc. Phil. Soc., Glasgow*, **13**, 464.

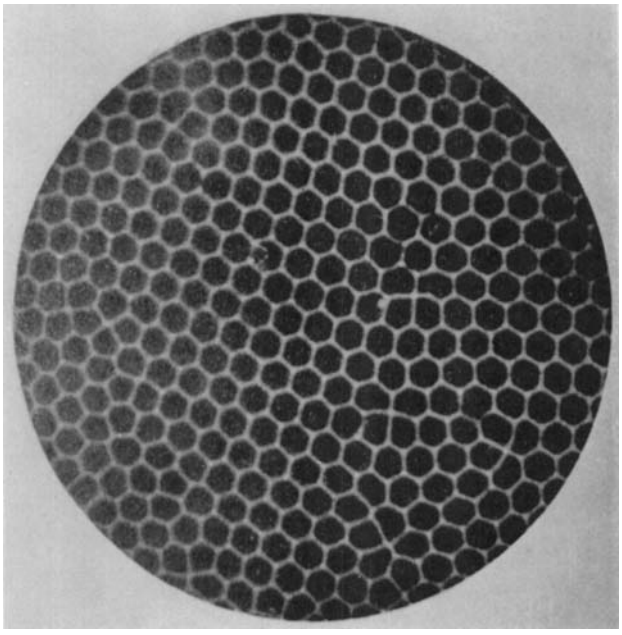

FIGURE 1. Cellular convection in a layer of spermaceti by Bénard. Diameter 32 mm (Avsec 1939).

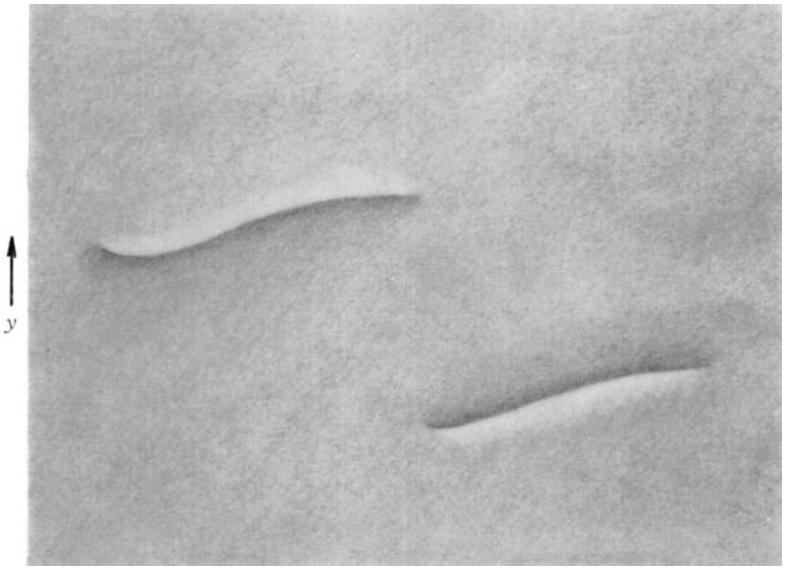

FIGURE 6. Distinction between 'hot lines' and 'cold lines' in schlieren image. Temperature extrema occur where there are sharp changes in image brightness.

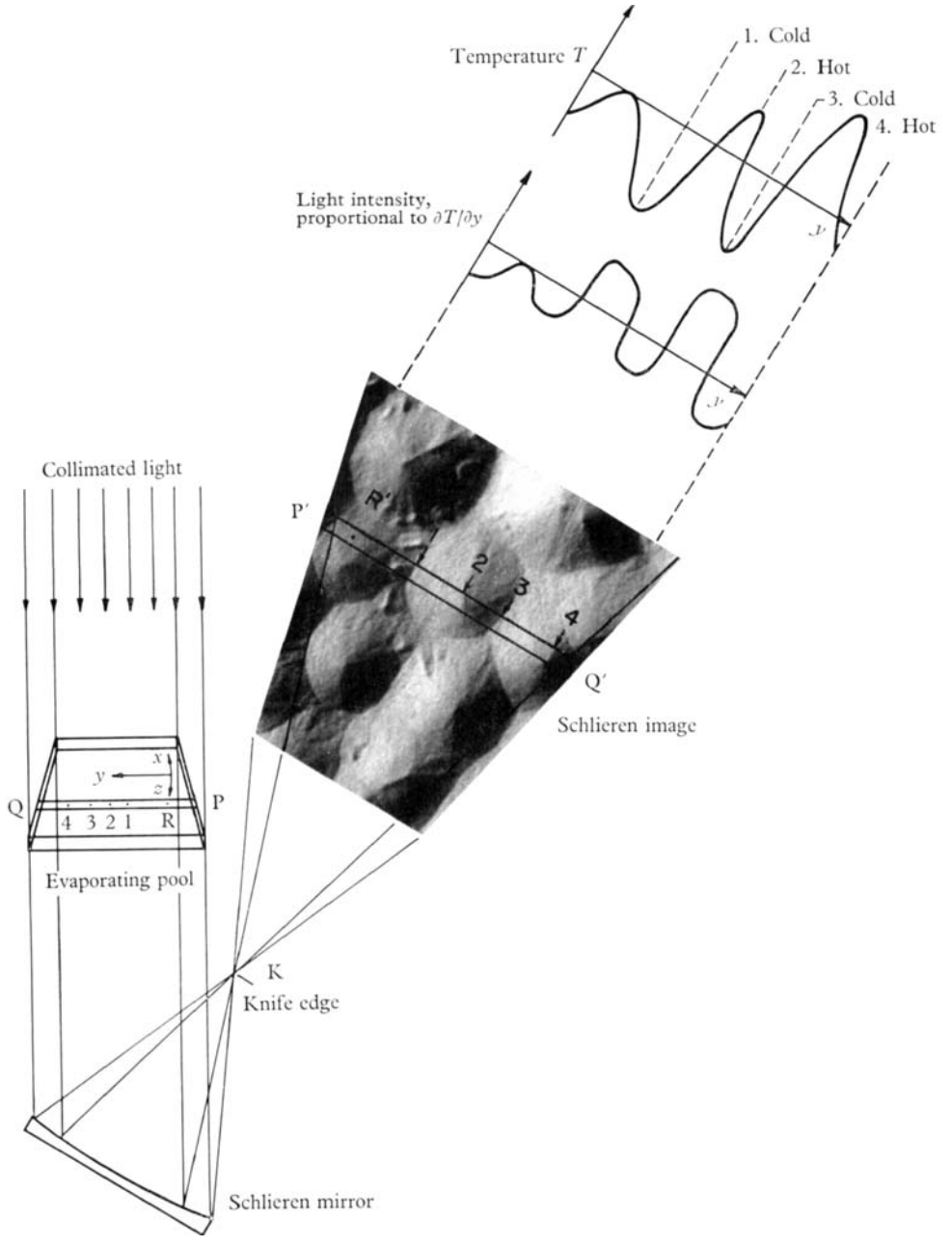

FIGURE 4. Interpretation of the schlieren image produced by a pool (depth 2 mm) of evaporating methanol. The distribution of light and dark regions in the image are qualitatively related to the temperature distribution in the liquid.

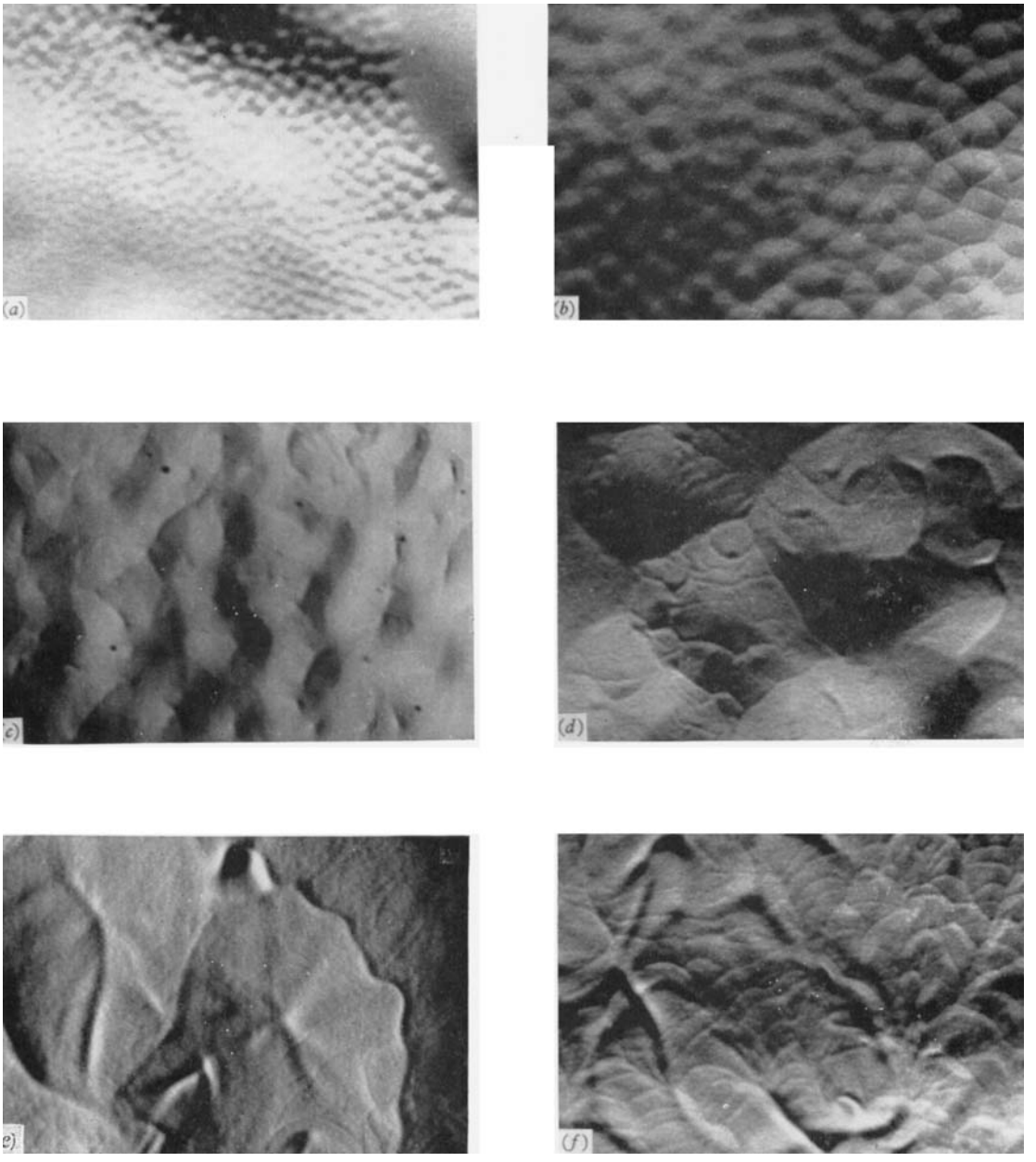

FIGURE 7. Schlieren top views of evaporation convection in pools of benzene. Magnification 1·8. (*a*) Depth 0·5 mm; (*b*) depth 1 mm; (*c*) depth 3 mm; (*d*) depth 4 mm; (*e*) depth 6 mm; (*f*) depth 9 mm.

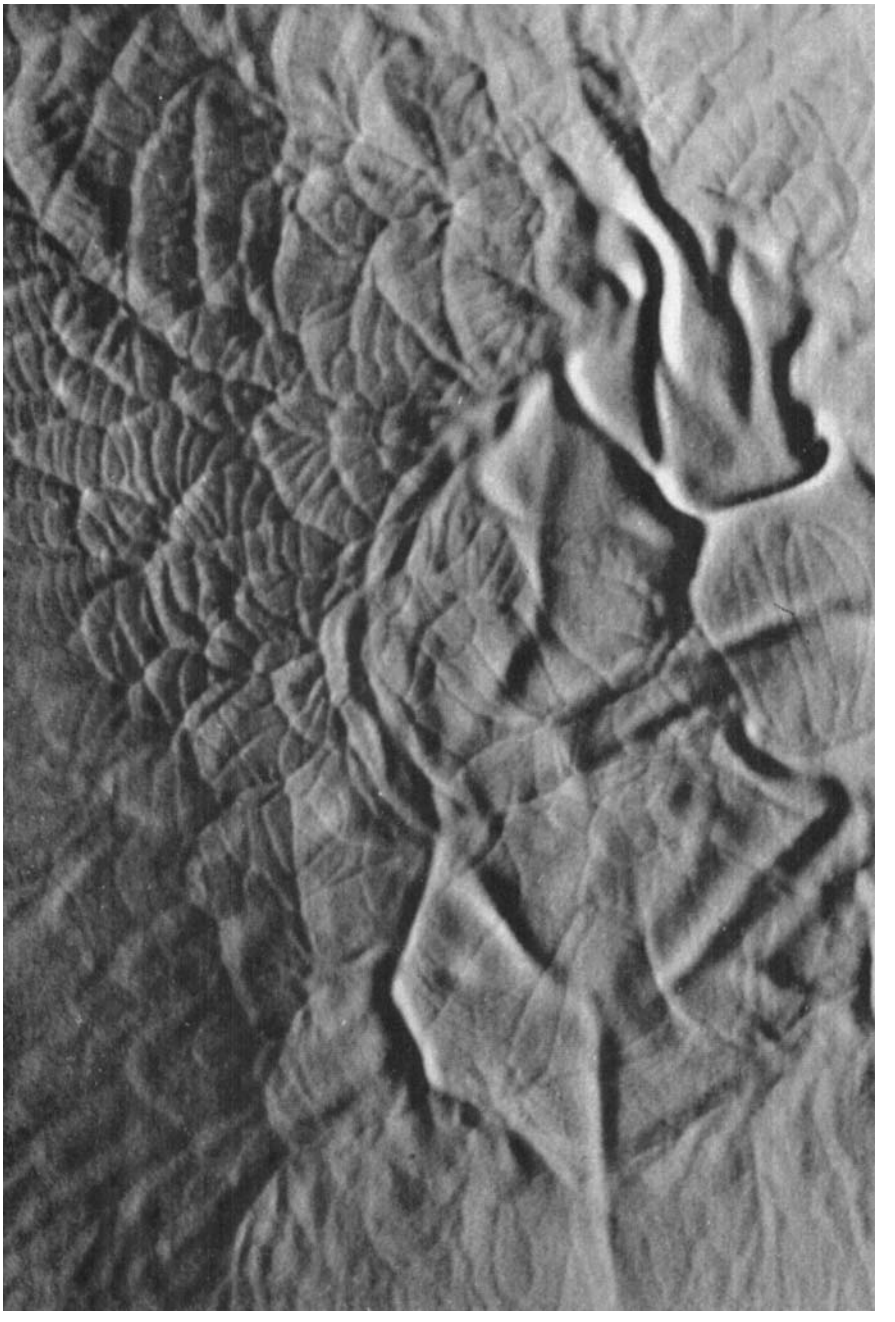

FIGURE 9. Fully developed convection pattern of streamers and ribs in a 10 mm deep pool of benzene. Magnification 3·5.

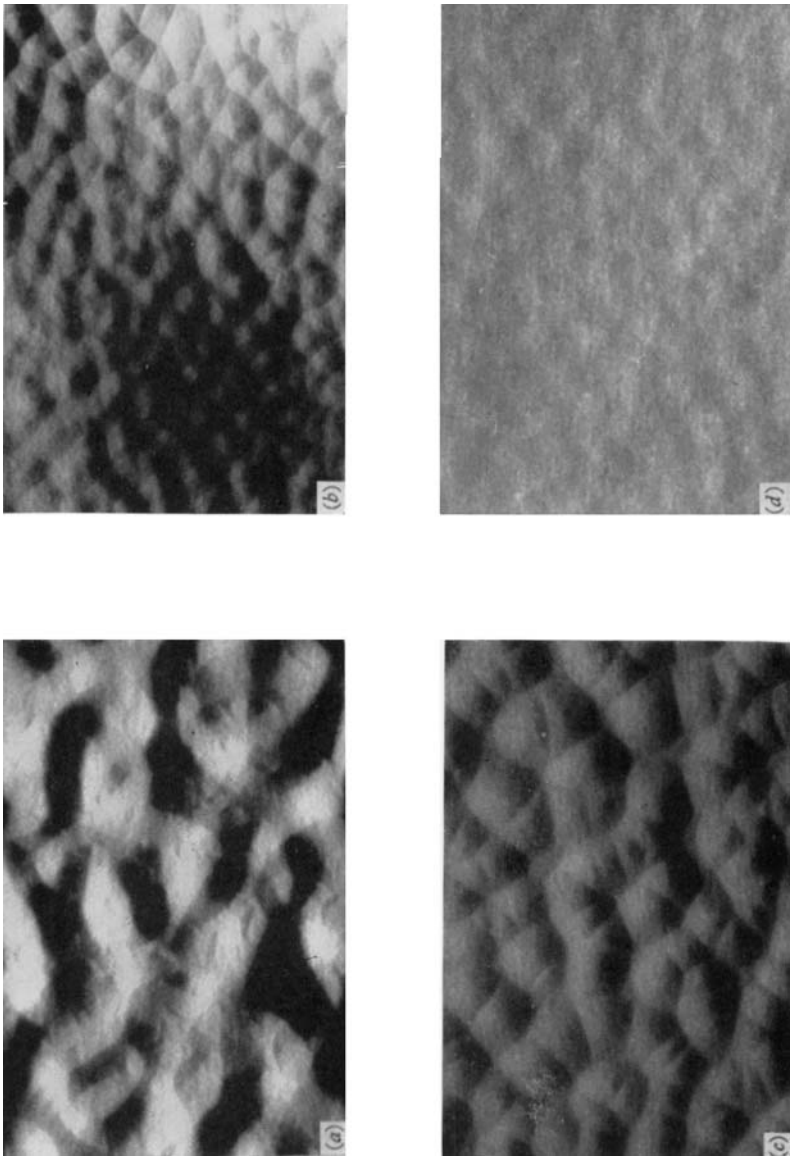

FIGURE 10. For legend see Plate 6.

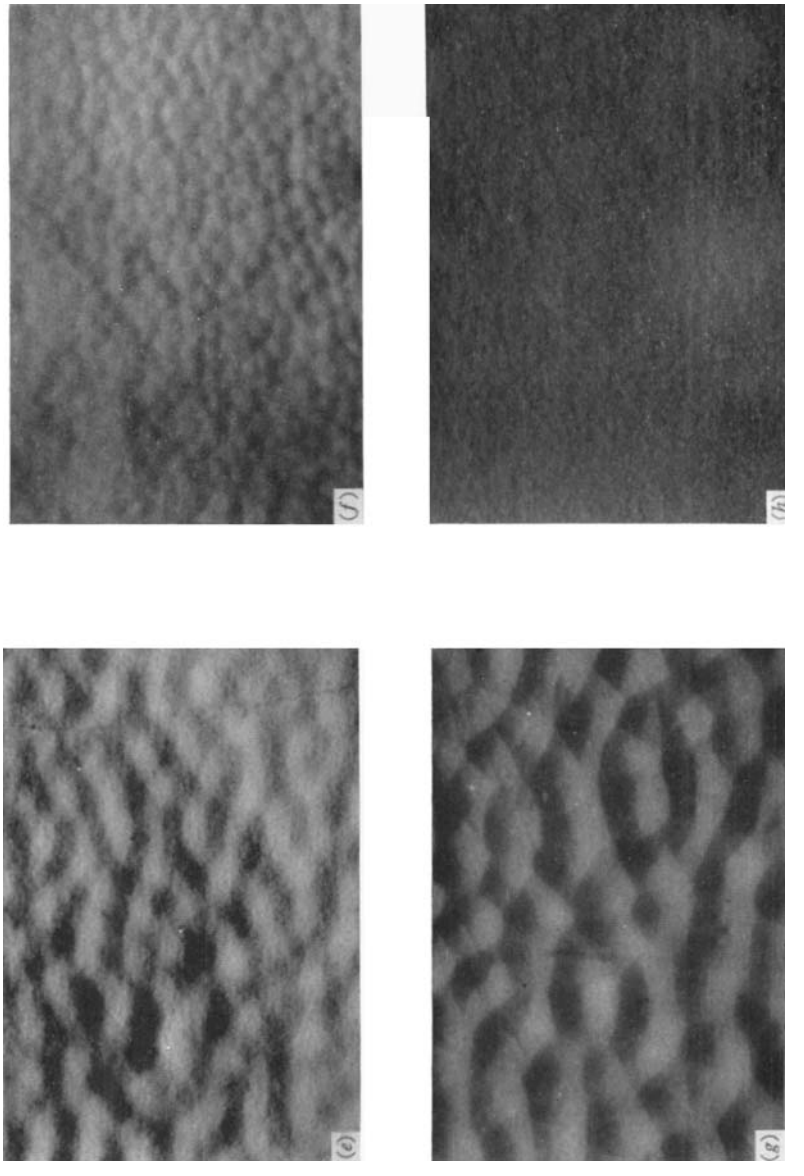

FIGURE 10. (*a*) Acetone; (*b*) benzene; (*c*) carbon tetrachloride; (*d*) 1,4-dioxane; (*e*) *n*-heptane; (*f*) isopropanol; (*g*) methanol; (*h*) water (no convection). Evaporative convection in 1 mm deep pools of various liquids. Magnification 1·8.

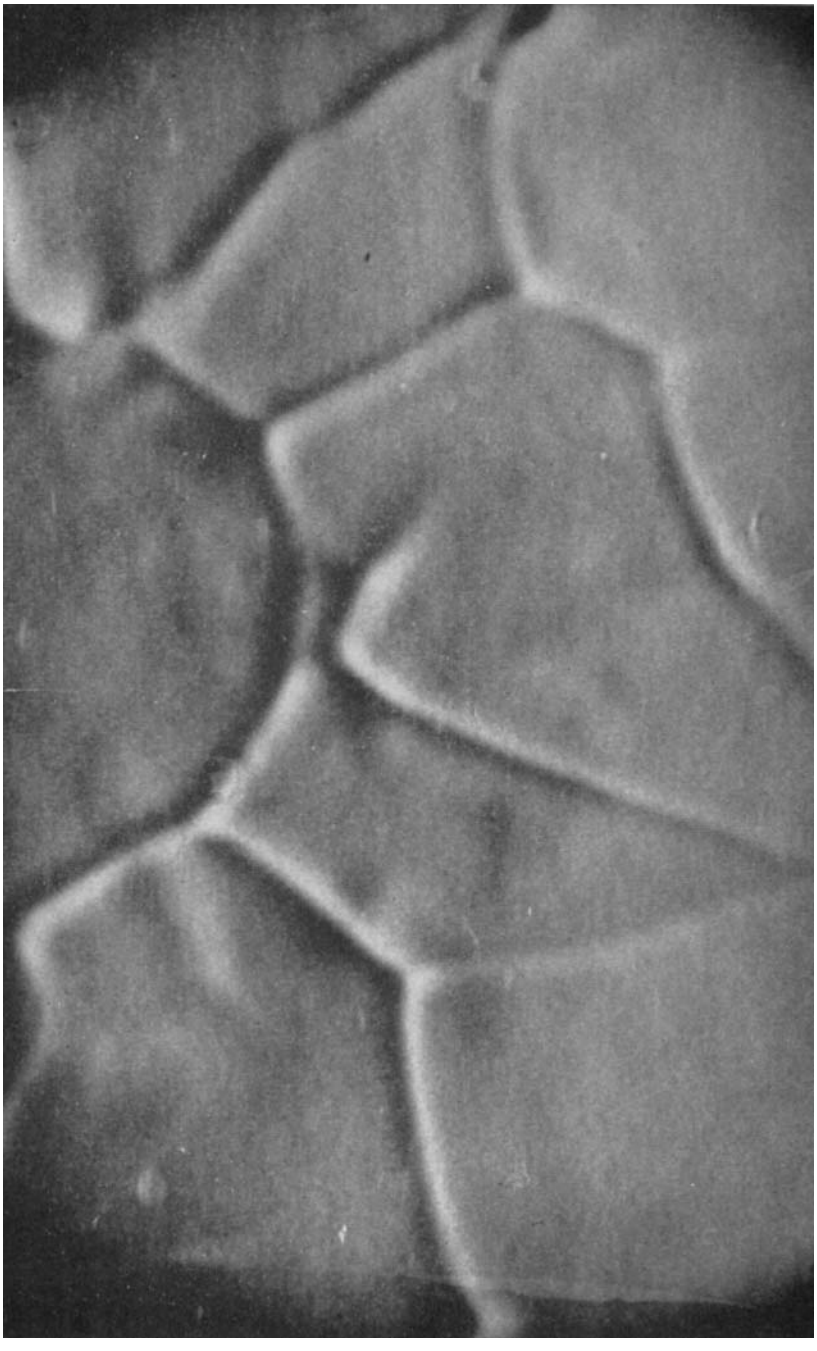

FIGURE 11. Evaporative convection in a 10 mm deep pool of water. Magnification 3·5.

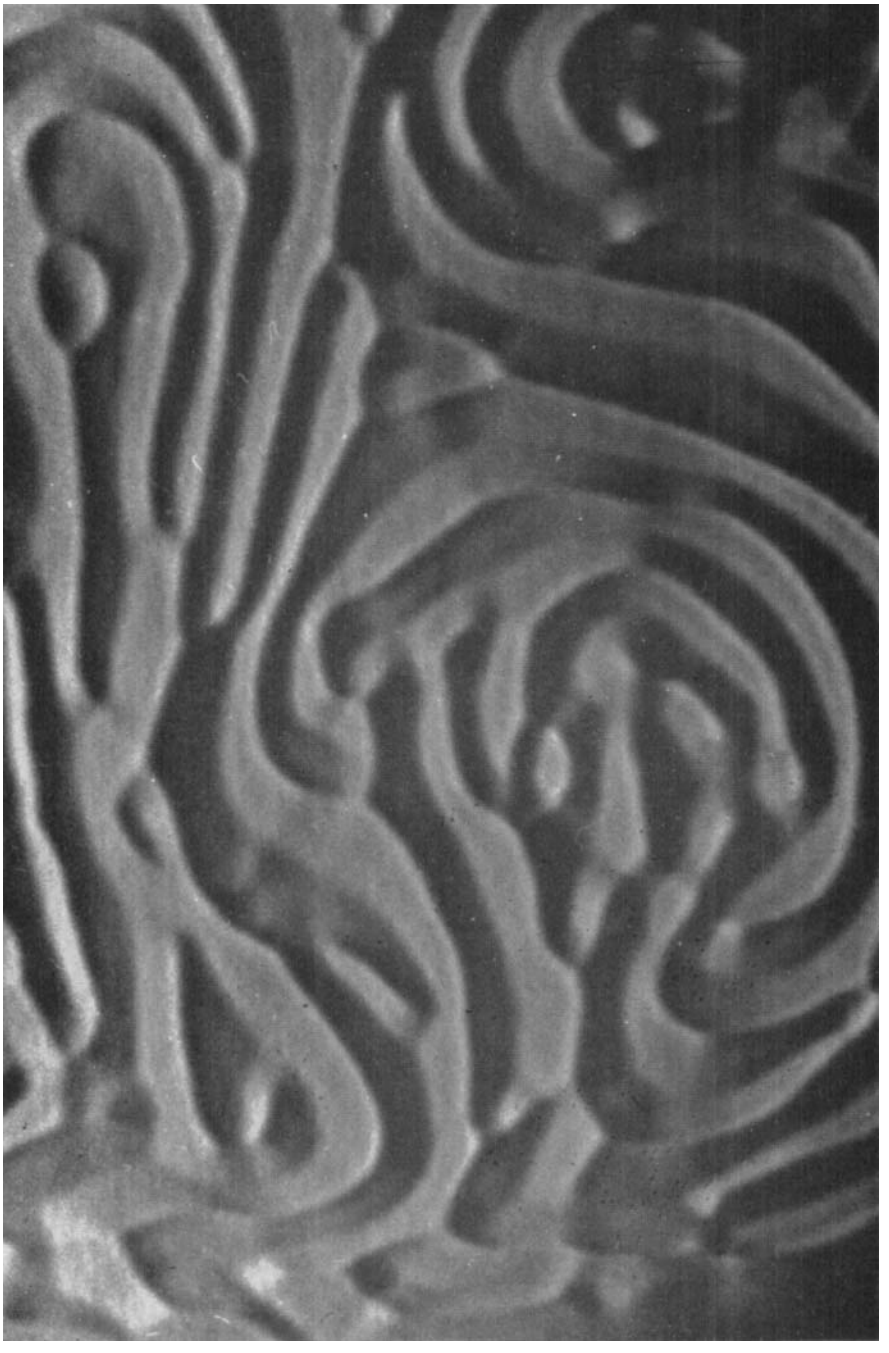

FIGURE 14. Vermiculated roll cells in a 3 mm deep pool of carbon tetrachloride. Surface is contaminated with a trace amount of paraffin wax. Magnification 3·5.

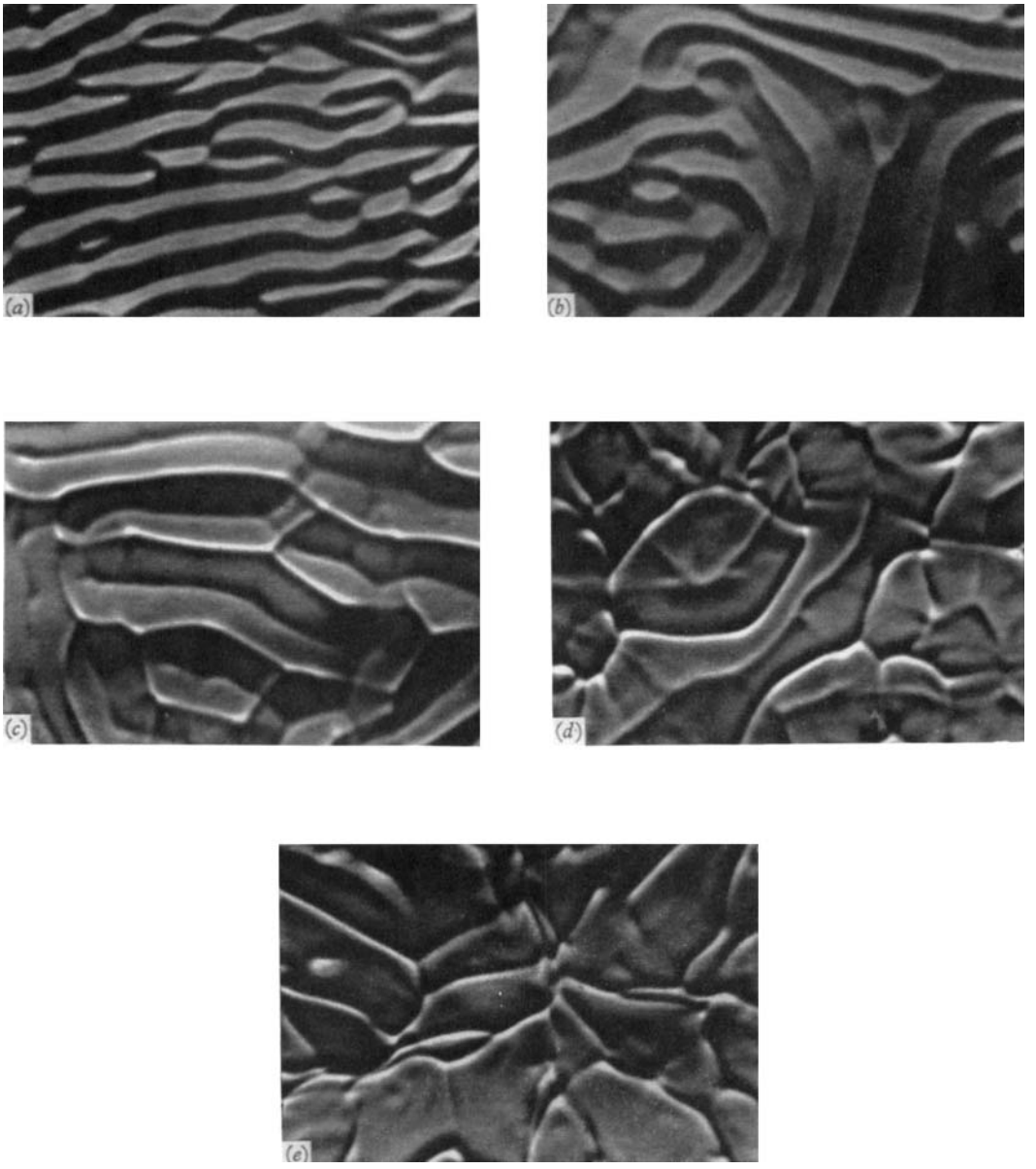

FIGURE 16. Evaporative convection in pools of carbon tetrachloride with surface contamination. Magnification 1·8. (*a*) Depth 2 mm; (*b*) depth 3 mm; (*c*) depth 4 mm; (*d*) depth 6 mm; (*e*) depth 10 mm.

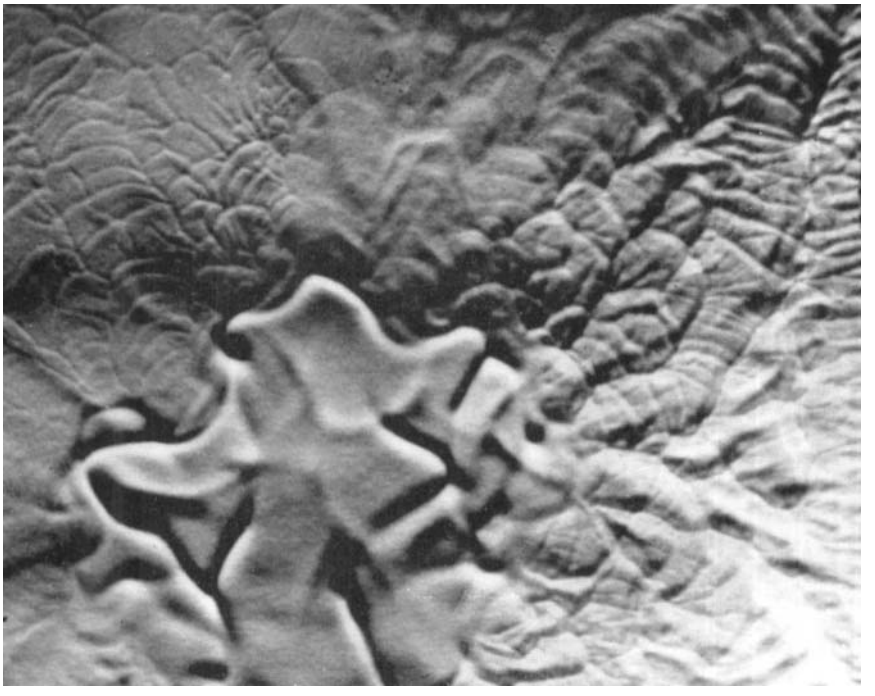

FIGURE 17. Evaporative convection in an 8 mm deep pool of benzene with a partially contaminated surface. Magnification 1·8.

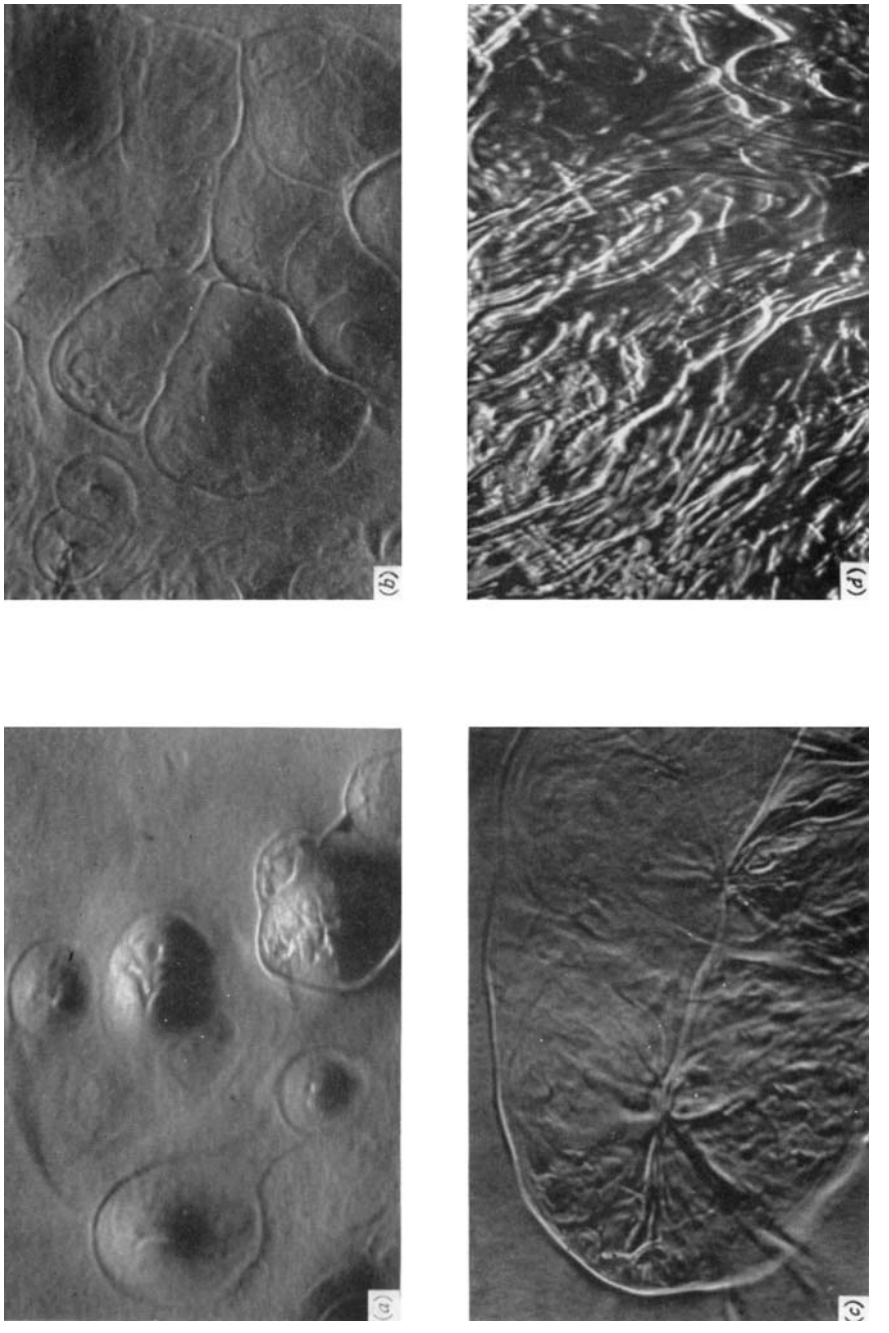

FIGURE 18. Convection accompanying the desorption of 1,4-dioxane from pools of an equi-volume solution of 1,4-dioxane and water. Magnification 1·8. (*a*) Depth 1 mm; (*b*) depth 2 mm; (*c*) depth 4 mm; (*d*) depth 10 mm.

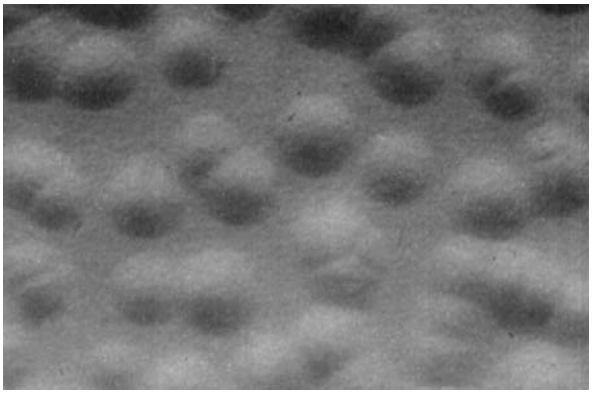

FIGURE 13. Isolated cells in a 1 mm layer of evaporating carbon tetrachloride whose surface is covered with a film of oleic acid. Magnification 1·8.

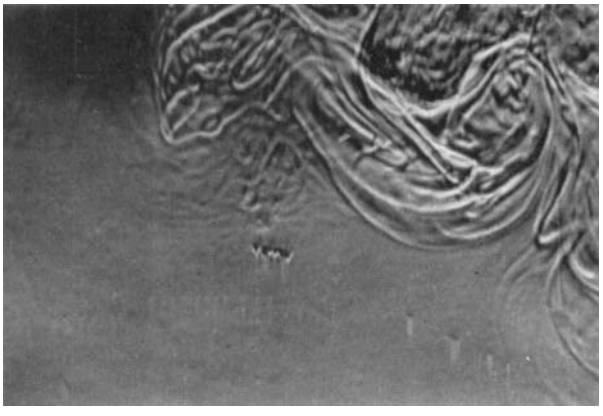

FIGURE 19. Schizoid flow in a 10 mm deep layer of a solution of dioxane (50 %) and water (50 %). Dioxane is desorbing from the solution, whose surface is contaminated with a trace of paraffin wax. Photograph taken 5 min from beginning of desorption. Within an hour the liquid will become totally placid. Magnification 1·8.

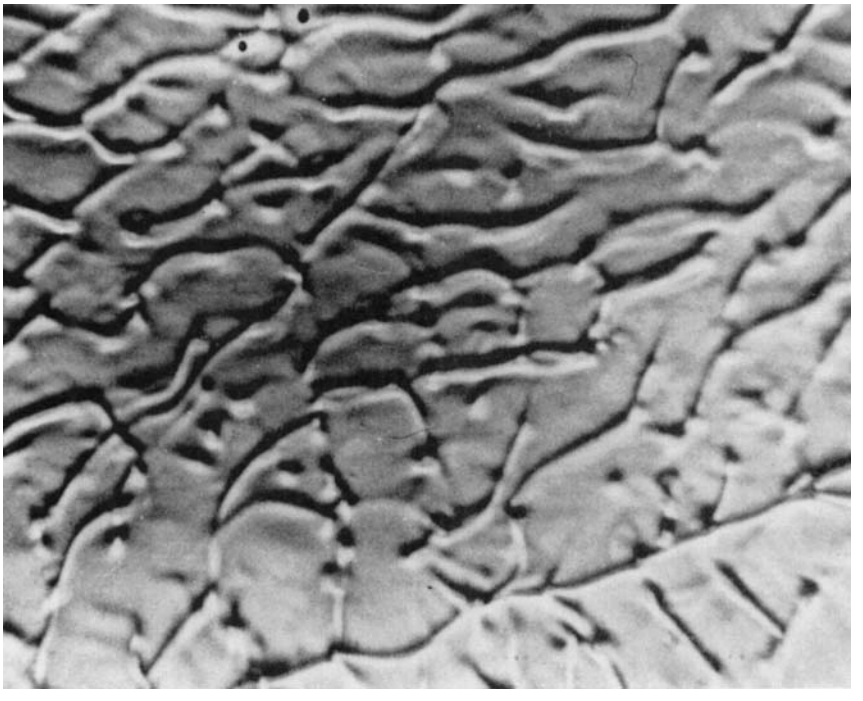

FIGURE 20. Water desorbing from a 10 mm deep pool composed of equal volumes of water and 1,4-dioxane. Magnification 1·8.

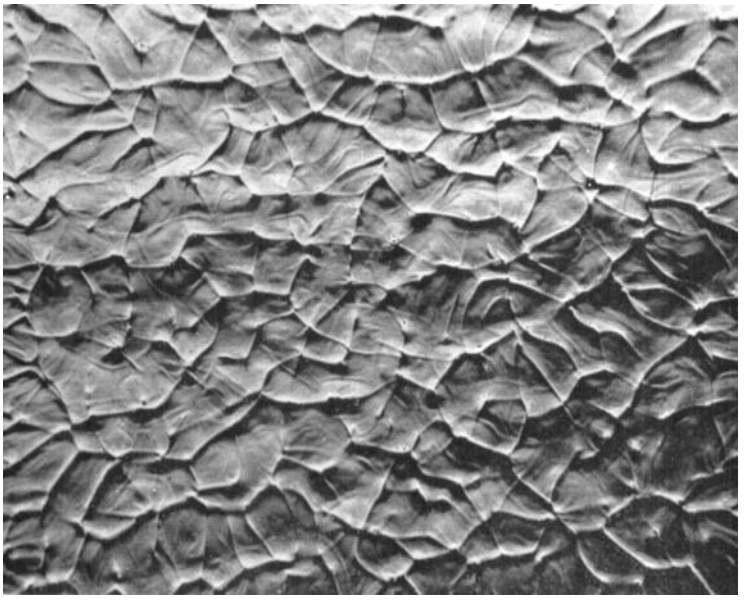

FIGURE 21. Acetone desorbing from a 7 mm deep pool composed of equal volumes of acetone and carbon tetrachloride.

FIGURE 22. Isopropanol desorbing from a 2 mm deep pool composed of equal volumes of isopropanol and water. Subject to both surface-tension- and buoyancy-driven convection. Magnification 1·8.

FIGURE 23. Benzene desorbing from a 6 mm deep pool composed of equal volumes of benzene and a silicone oil (Dow Corning Fluid 200–50). The system is subject only to buoyancy-driven convection. Magnification 1·8.

FIGURE 24. Benzene desorbing from an 8 mm deep pool composed of equal volumes of benzene and white oil. The system is subject only to surface-tension-driven convection. Magnification 1.8.